Nano Res. 2011, 4(11): 1110–1116
DOI 10.1007/s12274-011-0158-1
Research Article

ISSN 1998-0124
CN 11-5974/O4

Temperature-Dependent Photoconductance of Heavily Doped ZnO Nanowires

Dongdong Li[1], Liang Zhao[1], Ruqian Wu[2], Carsten Ronning[3], and Jia G. Lu[1] (✉)

[1] Departments of Physics and Electrophysics, University of Southern California, Los Angeles, CA 90089, USA
[2] Department of Physics, University of California, Irvine, CA 92697, USA
[3] Institute of Solid State Physics, University of Jena, D-07743, Germany

Received: 12 February 2011 / Revised: 6 June 2011 / Accepted: 8 June 2011

ABSTRACT

Ga-doped ZnO nanowires have been synthesized by a pulsed laser chemical vapor deposition method. The crystal structure and photoluminescence spectra indicate that the dopant atoms are well integrated into the ZnO wurtzite lattice. The photocurrent properties at different temperatures have been systematically investigated for nanowires configured as a three-terminal device. Among the experimental highlights, a pronounced semiconductor-to-metal transition occurs upon UV band-to-band excitation. This is a consequence of the reduction in electron mobility arising from the drastically enhanced Coulomb interactions and surface scattering. Another feature is the reproducible presence of two resistance valleys at 220 and 320 K upon light irradiation. This phenomenon originates from the trapping and detrapping processes in the impurity band arising from the native defects as well as the extrinsic Ga dopants. This work demonstrates that due to the dimensional confinement in quasi-one-dimensional structures, enhanced Coulomb interaction, surface scattering, and impurity states can significantly influence charge transport.

KEYWORDS

ZnO, nanowire, doping, semiconductor-to-metal transition, photoconductance, impurity states

1. Introduction

Strong research effort continues in the investigation of zinc oxide nanowires due to their remarkable functionalities. In order to explore their potential applications as the building blocks for nanoscale electronic and photonic devices, it is crucial to investigate in depth their fundamental properties [1]. ZnO is an *n*-type semiconductor with a wide band gap (3.37 eV), a large exciton binding energy (60 meV), and substantial native defects [2, 3]. There has been extensive work on extrinsic doping of ZnO nanostructures, with various elements including Mg [4, 5], Ga [6, 7], In [7, 8], Sn [7], Ni [9], Al [10], Mn [11], and Co [12], with the goal of tuning their structural, optical, electrical, and magnetic properties. Due to the abundant impurity states, the mechanisms of photoconduction are much more complex than simple generation of electron–hole pairs across the direct band gap. Therefore, it is challenging to understand the photoelectrical properties of these nanowires, and the contribution from the defect levels. In addition, it

Address correspondence to jia.grace.lu@usc.edu

is of fundamental interest to study size confinement and semiconductor-to-metal transitions in heavily doped systems. To elucidate these effects, we have used Ga doped ZnO (ZnO:Ga) as a study platform. Single crystalline ZnO:Ga nanowires were synthesized by pulsed laser chemical vapor deposition (PLCVD). Temperature-dependent electrical conduction measurements were performed under light irradiation. Combined with the photoluminescence spectra, the experimental results provide new insights into the mechanisms of carrier excitation, generation, trapping, and detrapping processes.

2. Experimental

Pure zinc powder (99.99%) was placed in the center of a horizontal tube furnace, while Ga metal is loaded at the up-stream of the quartz tube. The furnace was heated up to 650 ℃ in 15 min. The Ga source was constantly ablated by Nd:YAG (yttrium aluminum garnet) laser pulses. Oxygen (23 ppm) diluted by argon was used as carrier gas at a flow rate of 220 standard cubic centimeters per minute (sccm) under ambient pressure. ZnO:Ga nanowires were then collected on tin-coated (5 nm thick as catalyst) silicon substrates via the catalytic vapor–liquid–solid process [13].

The as-synthesized nanowires were suspended in isopropyl alcohol, and then spread onto degenerately doped Si substrates capped with a 500 nm SiO_2 layer at a controllable density. Photolithography followed by electrode deposition of Ti (5 nm)/Au (50 nm) was carried out to define contact patterns with a 2 μm inter-electrode distance. Post-thermal annealing was applied at 300 ℃ to further improve the electrode contacts. All the transport measurements were performed in vacuum under 10^{-6} Torr in a variable temperature cryostat.

3. Results and discussion

PLCVD is a robust method for *in situ* impurity doping of nanowires as shown in our previous work [8]. Figure 1(a) shows the as-obtained ZnO:Ga nanowires. The corresponding energy dispersive X-ray (EDX) spectrum in the inset shows that the atomic ratio of Ga to Zn is ~0.8%.

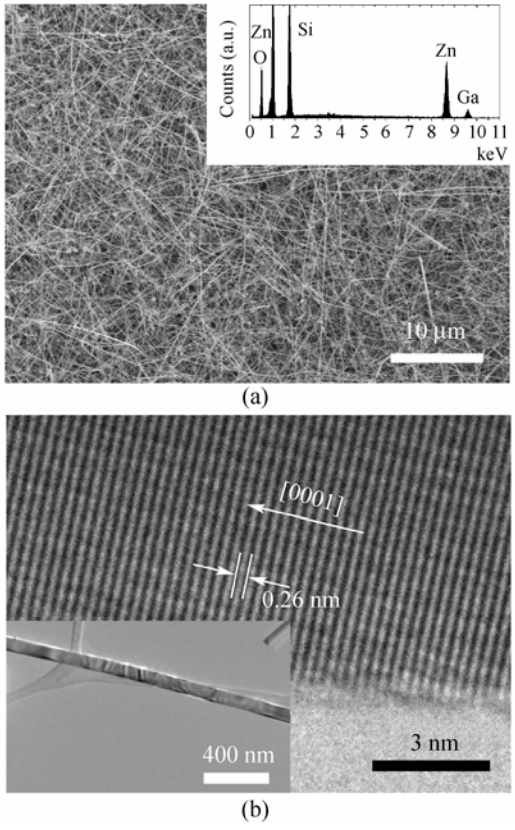

Figure 1 (a) SEM image of ZnO:Ga nanowires collected on a Si substrate, and the corresponding EDX spectrum (inset) of the ZnO:Ga nanowires. (b) The HRTEM and TEM (inset) images of an individual ZnO:Ga nanowire, labeling the [0001] growth direction along the wire axis

Figure S-1 in the Electronic Supplementary Material (ESM) displays the EDX elemental mapping images, showing a uniform distribution of Ga atoms well incorporated in the nanowires. Transmission electron microscopy (TEM) and high resolution TEM (HRTEM) performed on an individual nanowire (Fig. 1(b)) verify the high crystalline quality of the doped wurtzite ZnO [1]. The inter-planar spacing of 0.26 nm can be indexed to the (0001) plane, indicating that the nanowires grow along the *c*-axis and the dopant atoms have been well integrated into the wurtzite crystal lattice.

The electrical transport properties were first investigated for single nanowires (~60 nm in diameter) in a four-probe configuration with a global back gate on Si substrates, capped with a 500 nm SiO_2 layer [8, 14]. Figure 2(a) shows the linear voltage–current (V–I) curves under different gate voltages (V_g) at 4.92 K, indicating good ohmic contacts between the nanowire and Ti/Au electrodes.

Figure 2(b) displays the I_{DS}–V_g curves with different bias voltages at 4.92 K in dark conditions, indicating an *n*-type semiconductor behavior. The back gate capacitance of this nanowire can be estimated by $C = \frac{2\pi\varepsilon_0\varepsilon_r L}{\ln[(2h+r)/r]}$, where r is the radius of the nanowire, L the length of the channel ($L \gg r$), ε_r (~2.66) the effective gate dielectric constant [15], and h the thickness of SiO_2 film. The capacitance per unit length is around 0.42 pF/cm. The field-effect model has often been used to estimate the charge concentration in semiconductors by assuming constant mobility μ as the gate voltage V_g varies [16]. However, this assumption is not strictly valid in the case of degenerate carriers. As shown in Ref. [15], the conductivity σ varies with resistance R as $d\sigma/\sigma = -(dR/R) = (2/3)(dN/N)$, where N is the total number of carriers in the wire, and depends on V_g as $dN = C\,dV_g/e$. From the measurements at T = 4.9 K and V_{DS} = 0.2 V, the carrier concentration n in the dark (for the wire with L = 10 μm and r = 30 nm) was calculated to be ~8.12×10^{18} cm^{-3}. The corresponding transport characteristics under He–Ne laser (λ_{ph} = 632.8 nm, E_{ph} = 1.96 eV), and UV (λ_{UV} = 254.0 nm, E_{UV} = 4.88 eV) illumination are represented in Fig. S-2 in the ESM. The carrier concentrations were roughly estimated to be 1.78×10^{19} cm^{-3} and 6.88×10^{19} cm^{-3}, respectively. Under irradiation, excess electrons are excited to the conduction band by incident photons, and due to the slower surface desorption of oxygen in vacuum in ZnO nanowires [17, 18], the photogenerated electrons persist, giving rise to a charge accumulation.

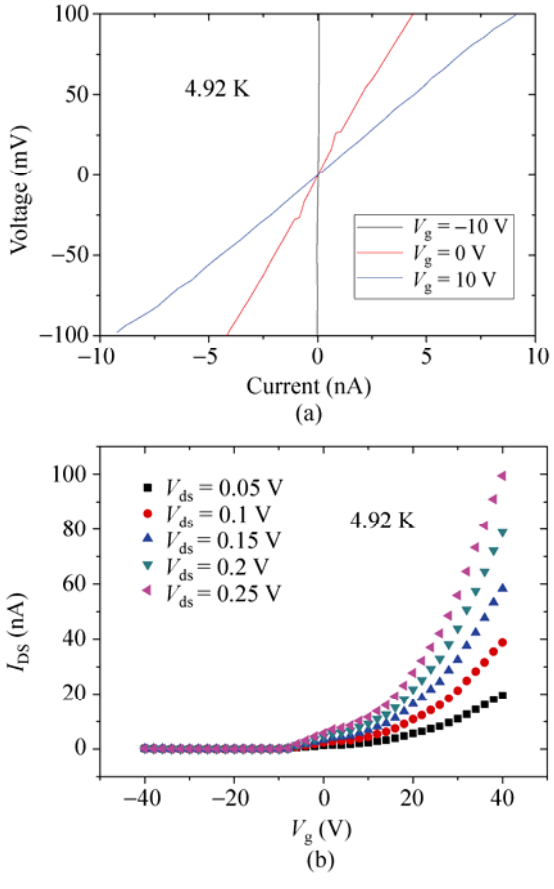

Figure 2 (a) Voltage–current curves obtained under different gate voltages (V_g = –10, 0, and 10 V). (b) I_{DS}–V_g characteristics under different bias voltages

Figure 3(a) shows the semilogarithmic plot of conductivity versus reciprocal temperature under dark conditions. It is known that the electrical transport behavior of undoped ZnO nanowires at relatively high temperature (above ~50 K) is mainly governed by thermal excitation [19, 20]. The linear region shows such an Arrhenius behavior which can be fitted with $\sigma \propto e^{-Ea/kT}$, where E_a, k (= 8.617×10^{-5} eV·K^{-1}) and T are the activation energy, Boltzmann constant and absolute temperature, respectively. The value of E_a extracted from the slope is ~20.8 meV, corresponding to the shallow donor levels arising from the native and extrinsic defects [21, 22].

Figure 3(b) plots the resistivity of a ZnO:Ga nanowire as a function of temperature under dark conditions, and illumination by a He–Ne laser (λ_{ph} = 632.8 nm, E_{ph} = 1.96 eV) and UV (λ_{UV} = 254.0 nm, E_{UV} = 4.88 eV). The phenomenon of persistent photoconductivity is typically observed in ZnO channels due to the shallow traps below the conduction band [23–25]. In order for the system to relax back to the initial state, after each variable temperature photoconductance measurement, the device was held in the dark chamber for up to three days under ambient environment. The resistivity behavior in the dark and under continuous laser excitation (the red curve in Fig. 3(b)) follow the semiconducting-like behavior, i.e. resistivity decreases with increasing temperature. In sharp contrast, under continuous UV illumination (the violet curve in Fig. 3(b)), the temperature-dependent resistivity changes dramatically to a metallic-like behavior. Considerable resistivity suppression is expected in semiconductors due to both thermal excitation and photogeneration; however, the surprising observation

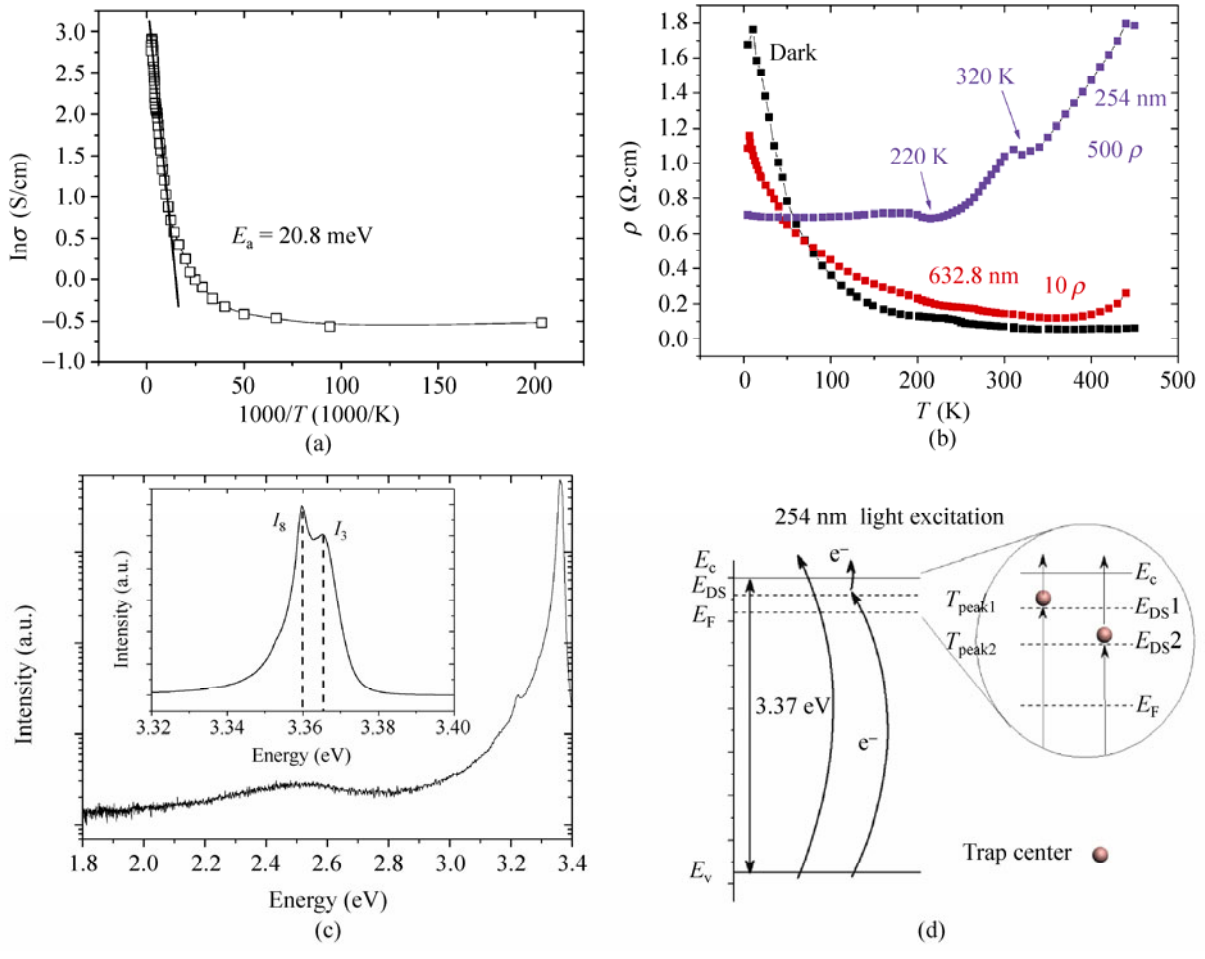

Figure 3 (a) Semilogarithmic plot of conductivity versus reciprocal temperature under dark conditions. (b) Temperature-dependent resistivity in the dark and under illumination at 632.8 and 254.0 nm. For the convenience of comparison on the same plot, the resistivity data under visible laser and UV irradiation are multiplied by 10 and 500, respectively. (c) PL spectrum of ZnO:Ga nanowires measured at 13 K, showing a weak green luminescence band at ~2.5 eV (496 nm). Inset: The high resolution plot focusing at the band-edge luminescence representing donor bound exciton emission. (d) Schematic band diagram of electron excitation under 254 nm UV (E_{ph} = 4.88 eV) illumination. The zoomed-in diagram shows the native and extrinsic impurity levels, giving rise to the corresponding resistance peaks due to trapping and detrapping processes

of a semiconductor-to-metal transition under UV light excitation above the band gap is an indication of significantly enhanced Coulomb interactions and surface scattering in the quasi-1D channels.

In addition, two distinct resistivity valleys are clearly observed at 220 and 320 K. Careful examination shows that the 632 nm laser illumination also induce formation of these resistivity valleys at the same temperatures, although the effect is of much smaller magnitude than with the 254 nm UV irradiation. To cross check the data, additional ZnO:Ga nanowires were measured under the same conditions, and showed two similar resistivity valleys at 220 and 315 K (see Fig. S-3 in the ESM). Reproducible formation of these two valleys signifies sharp transitions at two electronic states, and they are attributed to the existence of impurity levels below the conduction band edge [2], leading to charge trapping and detrapping processes.

To verify this contribution from the impurity states, photoluminescence (PL) measurements using He–Cd laser (λ = 325 nm) incident excitation were conducted in order to compare with the photoconductance data.

Low temperature PL is one of the best methods to probe radiative defect states. The PL spectrum in Fig. 3(c) displays a weak green luminescence band at around 2.5 eV. The green emission originates from the presence of deep lying defect states such as oxygen vacancies and structural defects, as in the undoped ZnO system [26–28]. A weak UV emission shoulder at 3.2206 eV (λ = 384 nm) can be reproducibly observed in the PL data, which is attributed to the donor–acceptor pair emissions in ZnO [29, 30]. An intense luminescence of donor bound excitons around the band edge remains sharp as in undoped emission PL (data not shown) [28, 31], suggesting that the Ga dopants have been well integrated into the ZnO lattice. On closer inspection of the bound exciton emission (inset of Fig. 3(c)), the peak splits into two distinct lines, showing that the Ga doping induces shallow donor levels [32]. The small peak at 3.3654 eV is caused by ionized donor bound excitons, typically assigned as the I_3 line [31]. The prominent emission line at 3.3597 eV can be indexed to the I_8 line, attributed to the exciton emission bound to Ga donors [31, 33, 34].

By comparing the photoconductance and photoluminescence measurements, the conduction mechanisms in ZnO nanowires can be understood. Both thermal and optical excitations affect the conduction in the nanowire. Under continuous UV irradiation, metallic behavior was observed. The strong Coulomb interactions between the dramatic increase in the number of charge carriers causes the resistance to increase as the temperature rises. The resistance valleys result from the defect levels. To illustrate the process, Fig. 3(d) shows the schematic band diagram of ZnO:Ga and the effect under 254 nm UV illumination (4.88 eV). E_V, E_C, and E_{DS} denote respectively valence band edge, conduction band edge, and shallow defect levels which arise from the native defects and external impurity dopants. The E_{DS} levels serve as trapping and detrapping centers. At low temperatures, the photo-excited electrons from valence band get trapped in the emptied localized defect states (E_{DS} levels). As the temperature increases to ~220 K, the electrons occupying the $E_{DS}1$ state become detrapped and thermally excited to the conduction band, causing an increase in the electron concentration, giving rise to the first resistivity valley. The second valley occurs as the trapped electrons are excited from the $E_{DS}2$ level to the conduction band. Considering the consistent valley positions at 220 and 320 K, the two E_{DS} levels can be estimated to be 19.0 and 27.6 meV below the conduction band (Fig. 3(d)), based on the thermal excitation energies extracted from conductivity versus reciprocal temperature data. In addition, the difference between the two defect levels (8.6 meV) falls in the range of the difference between the I_3 and I_8 photoemission peaks (5.7 meV). This indicates that these resistivity valleys originate from the shallow defect states due to native and Ga donors. As mentioned before, the resistivity valleys are also observed at the same temperatures under laser illumination (632.8 nm, E_{ph} = 1.96 eV). However, the effect is naturally much diminished due to the insufficient energy provided to excite the electrons from the valence band to the E_{DS} levels. Yet ZnO is known to have deep-lying impurity states due to oxygen vacancies and structural defects (corresponding to the green luminescence in its PL spectrum), and laser irradiation can excite electrons in these impurity states up to the shallow states below the conduction band edge. Thus, based on the same trapping and detrapping mechanisms, this gives rise to the resistance valleys as temperature increases.

4. Conclusions

ZnO:Ga nanowires synthesized by the PLCVD method exhibit high crystal quality with well incorporated Ga dopants. Careful measurements conducted on the nanowires revealed their structural, electrical, and optical properties. Among the observation highlights, a pronounced semiconductor-to-metal transition takes place upon UV irradiation above the band gap, accompanied by the presence of two reproducible valleys in temperature-dependent photoconductance measurements. Combined with the information from the photoluminescence spectra, the resistance variation can be ascribed to the effects of charge trapping and detrapping processes at the shallow donor levels from native defects and impurity dopants. This work demonstrates that due to the dimensional confinement and enhanced surface scattering in quasi-1D structures, the localized impurity states give rise to a rich variety of conduction mechanisms.

Acknowledgements

This material is based upon work partially supported by the Center for Energy Nanoscience funded by the U. S. Department of Energy, Office of Science, Energy Frontier Research Center (EFRC) program under Award Number DE-SC0001013. D. L. is grateful for support from the Science and Technology Commission of Shanghai Municipality (China, grant number: 10DZ1210300, 11QA1406400, and 11ZR1436300). The current address of D. L. is Division of Energy and Environmental Research, Shanghai Advanced Research Institute, Chinese Academy of Sciences, Shanghai 201203, China. R. W. acknowledges support from DOE grant No. DE-FG02-05ER46237.

Electronic Supplementary Material: Supplementary material (EDX elemental mapping images, transport characteristics under light illumination and transport properties of another individual ZnO:Ga nanowire) is available in the online version of this article at http://dx.doi.org/10.1007/s12274-011-0158-1 and is accessible free of charge.

References

[1] Lu, J. G.; Chang, P. C.; Fan, Z. Y. Quasi-one-dimensional metal oxide materials—Synthesis, properties and applications. *Mater. Sci. Eng. R.* **2006**, *52*, 49–91.

[2] Hoyer, P.; Weller, H. Potential-dependent electron injection in nanoporous colloidal ZnO films. *J. Phys. Chem.* **1995**, *99*, 14096–14100.

[3] Hotchandani, S.; Kamat, P. V. Photoelectrochemistry of semiconductor ZnO particulate Films. *J. Electrochem. Soc.* **1992**, *139*, 1630–1634.

[4] Ju, S.; Li, J. Y.; Pimparkar, N.; Alam, M. A.; Chang, R. P. H.; Janes, D. B. *N*-type field-effect transistors using multiple Mg-doped ZnO nanorods. *IEEE T Nanotechnol.* **2007**, *6*, 390–395.

[5] Pan, H.; Zhu, Y. W.; Sun, H.; Feng, Y. P.; Sow, C. H.; Lin, J. Y. Electroluminescence and field emission of Mg-doped ZnO tetrapods. *Nanotechnology* **2006**, *17*, 5096–5100.

[6] Yuan, G. D.; Zhang, W. J.; Jie, J. S.; Fan, X.; Tang, J. X.; Shafiq, I.; Ye, Z. Z.; Lee, C. S.; Lee, S. T. Tunable *n*-type conductivity and transport properties of Ga-doped ZnO nanowire arrays. *Adv. Mater.* **2008**, *20*, 168–173.

[7] Bae, S. Y.; Na, C. W.; Kang, J. H.; Park, J. Comparative structure and optical properties of Ga-, In-, and Sn-doped ZnO nanowires synthesized via thermal evaporation. *J. Phys. Chem. B* **2005**, *109*, 2526–2531.

[8] Thompson, R. S.; Li, D.; Witte, C. M.; Lu, J. G. Weak localization and electron–electron interactions in indium-doped ZnO nanowires. *Nano Lett.* **2009**, *9*, 3991–3995.

[9] He, H.; Lao, C. S.; Chen, L. J.; Davidovic, D.; Wang, Z. L. Large-scale Ni-doped ZnO nanowire arrays and electrical and optical properties. *J. Amer. Chem. Soc.* **2005**, *127*, 16376–16377.

[10] Yamamoto, T.; Katayama-Yoshida, H. Solution using a codoping method to unipolarity for the fabrication of *p*-type ZnO. *Jpn. J. Appl. Phys. Part 2* **1999**, *38*, L166–L169.

[11] Salfi, J.; Philipose, U.; Aouba, S.; Nair, S. V.; Ruda, H. E. Electron transport in degenerate Mn-doped ZnO nanowires. *Appl. Phys. Lett.* **2007**, *90*, 032104.

[12] Liang, W. J.; Yuhas, B. D.; Yang, P. D. Magnetotransport in Co-doped ZnO nanowires. *Nano Lett.* **2009**, *9*, 892–896.

[13] Duan, X. F.; Lieber, C. M. General synthesis of compound semiconductor nanowires. *Adv. Mater.* **2000**, *12*, 298–302.

[14] Chang, P. C.; Fan, Z.; Chien, C. J.; Stichtenoth, D.; Ronning, C.; Lu, J. G. High-performance ZnO nanowire field effect transistors. *Appl. Phys. Lett.* **2006**, *89*, 133113.

[15] Thompson, R. S.; Li, D. D.; Witte, C. M.; Lu, J. G. Weak localization and electron–electron interactions in indium-doped ZnO nanowires. *Nano Lett.* **2009**, *9*, 3991–3995.

[16] Martel, R.; Schmidt, T.; Shea, H. R.; Hertel, T.; Avouris, P. Single- and multi-wall carbon nanotube field-effect transistors. *Appl. Phys. Lett.* **1998**, *73*, 2447–2449.

[17] Fan, Z. Y.; Wang, D. W.; Chang, P. C.; Tseng, W. Y.; Lu, J. G. ZnO nanowire field-effect transistor and oxygen sensing property. *Appl. Phys. Lett.* **2004**, *85*, 5923–5925.

[18] Bao, J.; Shalish, I.; Su, Z.; Gurwitz, R.; Capasso, F.; Wang, X.; Ren, Z. Photoinduced oxygen release and persistent photoconductivity in ZnO nanowires. *Nanoscale Res. Lett.* **2011**, *6*, 404.

[19] Chang, P. C.; Lu, J. G. Temperature dependent conduction and UV induced metal-to-insulator transition in ZnO nanowires. *Appl. Phys. Lett.* **2008**, *92*, 212113.

[20] Chiu, S. P.; Lin, Y. H.; Lin, J. J. Electrical conduction mechanisms in natively doped ZnO nanowires. *Nanotechnology* **2009**, *20*, 015203.

[21] Look, D. C.; Hemsky, J. W.; Sizelove, J. R. Residual native shallow donor in ZnO. *Phys. Rev. Lett.* **1999**, *82*, 2552–2555.

[22] Seghier, D.; Gislason, H. P. Characterization of donor states in ZnO. *Physica B* **2007**, *401*, 404–407.

[23] Liao, Z. M.; Lu, Y.; Xu, J.; Zhang, J. M.; Yu, D. P. Temperature dependence of photoconductivity and persistent photoconductivity of single ZnO nanowires. *Appl. Phys. A–Mater.* **2009**, *95*, 363–366.

[24] Nayak, J.; Kasuya, J.; Watanabe, A.; Nozaki, S. Persistent photoconductivity in ZnO nanorods deposited on electro-deposited seed layers of ZnO. *J. Phys.–Condensed Matt.* **2008**, *20*, 195222.

[25] Ahn, S. E.; Ji, H. J.; Kim, K.; Kim, G. T.; Bae, C. H.; Park, S. M.; Kim, Y. K.; Ha, J. S. Origin of the slow photoresponse in an individual sol–gel synthesized ZnO nanowire. *Appl. Phys. Lett.* **2007**, *90*, 153106.

[26] Leiter, F. H.; Alves, H. R.; Hofstaetter, A.; Hofmann, D. M.; Meyer, B. K. The oxygen vacancy as the origin of a green emission in undoped ZnO. *Phys. Status Solidi B* **2001**, *226*, R4–R5.

[27] van Dijken, A.; Meulenkamp, E. A.; Vanmaekelbergh, D.; Meijerink, A. The kinetics of the radiative and nonradiative processes in nanocrystalline ZnO particles upon photo-excitation. *J. Phys. Chem. B* **2000**, *104*, 1715–1723.

[28] Stichtenoth, D.; Ronning, C.; Niermann, T.; Wischmeier, L.; Voss, T.; Chien, C. J.; Chang, P. C.; Lu, J. G. Optical size effects in ultrathin ZnO nanowires. *Nanotechnology* **2007**, *18*, 435701.

[29] Zhang, B. P.; Binh, N. T.; Segawa, Y.; Wakatsuki, K.; Usami, N. Optical properties of ZnO rods formed by metalorganic chemical vapor deposition. *Appl. Phys. Lett.* **2003**, *83*, 1635–1637.

[30] Yamamoto, A.; Satake, Y.; Atsuta, S.; Taguchi, Y.; Ishizumi, A. The origins of photoluminescence peaks in ZnO nanocrystals revealed by microscopic photoluminescence imaging spectroscopy. *J. Phys. Soc. Jpn.* **2010**, *79*, 054701.

[31] Meyer, B. K.; Alves, H.; Hofmann, D. M.; Kriegseis, W.; Forster, D.; Bertram, F.; Christen, J.; Hoffmann, A.; Strassburg, M.; Dworzak, M.; Haboeck, U.; Rodina, A. V. Bound exciton and donor-acceptor pair recombinations in ZnO. *Phys. Status Solidi B* **2004**, *241*, 231–260.

[32] Chang, P. C.; Chien, C. J.; Stichtenoth, D.; Ronning, C.; Lu, J. G. Finite size effect in ZnO nanowires. *Appl. Phys. Lett.* **2007**, *90*, 113101.

[33] Johnston, K.; Henry, M. O.; McCabe, D.; McGlynn, E.; Dietrich, M.; Alves, E.; Xia, M. Identification of donor-related impurities in ZnO using photoluminescence and radiotracer techniques. *Phys. Rev. B* **2006**, *73*, 165212.

[34] Ko, H. J.; Chen, Y. F.; Hong, S. K.; Wenisch, H.; Yao, T.; Look, D. C. Ga-doped ZnO films grown on GaN templates by plasma-assisted molecular-beam epitaxy. *Appl. Phys. Lett.* **2000**, *77*, 3761–3763.